International Journal of Geology, Earth & Environmental Sciences ISSN: 2277-2081 (Online)
An Online International Journal Available at http://www.cibtech.org/jgee.htm
2013 Vol.3 (2) May-August, pp.141-152/Szekielda et al.
Research Article

SPATIAL DISTRIBUTION PATTERNS OF CHLOROPHYLL-*A* AND SUSPENDED MATTER IN THE YANGTZE ESTUARY AND THE HANGZHOU BAY AS OBSERVED WITH THE HYPERSPECTRAL IMAGER FOR THE COASTAL OCEAN (HICO)

[*]Karl H. Szekielda[1], Wesley J. Moses[2], Jeffrey H. Bowles[2], Michael R. Corson[2], Ellen J. Wagner[2] and Rong R. Li[2]

[1]Naval Research Laboratory/ASEE Summer Senior Faculty Fellow, Hunter College, City University of New York, 695 Park Avenue, New York, NY 10021
[2]Naval Research Laboratory, 4555 Overlook Ave., SW, Washington, DC 20375
[*]Author for Correspondence

ABSTRACT
Data from the Hyperspectral Imager for the Coastal Ocean (HICO) were used to identify gradients and patchiness due to chl-*a* and suspended matter in the Yangtze Estuary and the Hangzhou Bay in China. HICO images were classified using the spectral analysis to identify frontal systems and areas of plankton patchiness in these water bodies. The results obtained from the analysis were compared with results obtained from previous studies conducted in these water bodies. The chl-*a* concentrations estimated from atmospherically corrected HICO images were comparable to chl-*a* concentrations measured *in situ* previously in this region. The spatial patterns of chl-*a* distribution derived from the HICO data matched well with the spatial patterns derived from a MODIS image acquired on the same day.

Key Words: *Yangtze, Remote Sensing, Suspended Matter, HICO, Supervised Classification*

INTRODUCTION
Estuarine and coastal waters represent complex ecosystems that play crucial roles in maintaining global biodiversity but have been under tremendous ecological stress due to natural as well as anthropogenic factors, and thus warrant regular monitoring of their biophysical conditions. In addition, there are also commercial and recreational interests to characterizing and monitoring the estuarine and coastal systems. For decades, airborne and spaceborne remote sensing have been very effective and successful tools for monitoring water bodies, particularly the open ocean waters. However, monitoring coastal waters has been more difficult and challenging than monitoring open ocean waters because of the optical complexity of the coastal waters and also the fact that coastal waters are spatially and temporally more dynamic (Davis *et al.,* 2007) than open ocean waters. Commonly used spaceborne multispectral ocean color sensors such as SeaWiFS (Sea-viewing Wide Field-of-view Sensor), MODIS (MODerate resolution Imaging Spectroradiometer) and MERIS (MEdium Resolution Imaging Spectrometer) do not have the necessary spectral (Chang *et al.,* 2004; Sydor *et al.,* 2004) or spatial resolution (Bissett *et al.,* 2004) for detailed coastal analysis.

Technological developments in instrumentation and data processing capabilities (Chang *et al.,* 2004) have enabled the development and use of hyperspectral sensors with contiguous narrow spectral bands and high spatial resolution, which are capable of measuring fine spectral and spatial information from coastal waters. The Naval Research Laboratory's Hyperspectral Imager for Coastal Oceans (HICO) is a spaceborne hyperspectral sensor, developed as a demonstration mission and designed specifically for characterizing the coastal environment (Korwan *et al.,* 2010; Lucke *et al.,* 2011). HICO is a pushbroom hyperspectral sensor onboard the International Space Station (ISS). The sensor is designed to have a high signal-to-noise ratio in the visible part of the electromagnetic spectrum, which is crucial for aquatic remote sensing. HICO is considered as a path-finding instrument for the application of larger off-nadir observations from space with the primary objective to meet the specifications for coastal ocean imaging. The instrument and its performance have been documented in detail by Lucke *et al.,* (2011), thus only a

few fundamentals of HICO need to be addressed in this study. The major channels of HICO cover a nominal wavelength range of 0.350–1.325 µm with 512 spectral pixels of which the spectral range from 0.400–0.900µm is the most suitable for coastal and marine regions. HICO also has a high-resolution mode of operation in which pixels are not binned at readout, so that the 1.91nm spectral sampling is preserved and is used only occasionally to check the sensor's spectral calibration. The ISS is presently at an orbital altitude of about 350 km with an inclination of about 51.6° and is estimated that HICO, with the present orbital configurations, can observe about 80% of the Earth's surface with scenes that typically cover 42km × 192km.

In this study, we illustrate the high spatial and spectral resolutions of HICO data in analyzing the effluent from the Yangtze River and identifying fronts and algal blooms in the Hangzhou Bay region adjoining the East China Sea.

General Hydrography of the East China Sea

The Yangtze River is the longest river in Asia and runs into the East China Sea. This coastal region is strongly influenced by seasonal variations in the effluent and sediment transport from the Yangtze River, as evidenced by changes in the salinity near the northeastern part of the bay (Su and Wang, 1989). It is estimated that the Yangtze River transports about 486×10^6 tons of sediments per year to the coastal area (Shen *et al.,* 1983). The mineral composition of the sediments in the Hangzhou Bay is found to be similar to that in the Yangtze Estuary (Yan and Hu, 1986). During the summer season, freshwater transport occurs northeast along the eastern Chinese coastal area with southerly winds, and moves eastward over 400 km offshore across the western shelf of the northern East China Sea (Asanuma *et al.,* 2008; Son *et al.,* 2006) with a sharp turning point within the near-shore region. In the months of April, May and September, the effluent transport occurs in the southeast direction. The turning patterns of the effluent are apparently associated with factors such as the amount of discharge from the Yangtze River, the portioning of the discharge through the branches of the estuary, the position and strength of the coastal current and/or the Taiwan Warm Current, and the wind stress.

The resulting effect of the various processes acting on the Yangtze River effluent is the development of a very complicated pattern of suspended and dissolved matter that leads to patchiness and formations of plumes that are characterized by a salinity of less than 30 psu, extending to about 100 km offshore in summer and about 50 km in winter (Limeburger *et al.,* 1983), and can be recognized by satellite imagery (Zheng and Klemas, 1982; Szekielda and McGinnis, 1991; Hickox *et al.,* 2000).

The Yangtze River effluent contains high concentrations of nitrogen as a result of agricultural activity in the catchment area and nutrient discharge from Shanghai. Physical and biochemical processes trigger rapid changes in the distribution of organic and inorganic matter in the effluent, resulting in algal blooms. Large scale distributions of harmful algal blooms, covering up to thousands of square kilometers off the Yangtze Estuary have been documented (Lu *et al.,* 2007; Chai *et al.,* 2006).

Observations with HICO

Two images acquired by HICO, on 20 October 2009 and 18 January 2010 (Figure 1), were analyzed to identify gradients, fronts, and patchiness in the distribution of suspended matter, and also to detect algal blooms. The images have a small area of overlap at $31^o15'$N, $122^o30'$E.

For satellite data covering turbid waters, where the 'black-pixel' assumption is invalid, reflectance in the short wave infrared (SWIR) region can be used to estimate the contribution from atmospheric aerosols to the total radiance (Wang and Shi, 2005) and thus correct the data for atmospheric effects. HICO however does not collect data in the SWIR region and a reliable atmospheric correction remains a difficult task. Therefore, the analysis of the distribution and structure of the sediment plume was done based on at-sensor radiance recorded by HICO. This approach, however, has certain limitations because radiance-based analysis cannot be uniformly extended across multi-temporal images acquired under different illumination conditions.

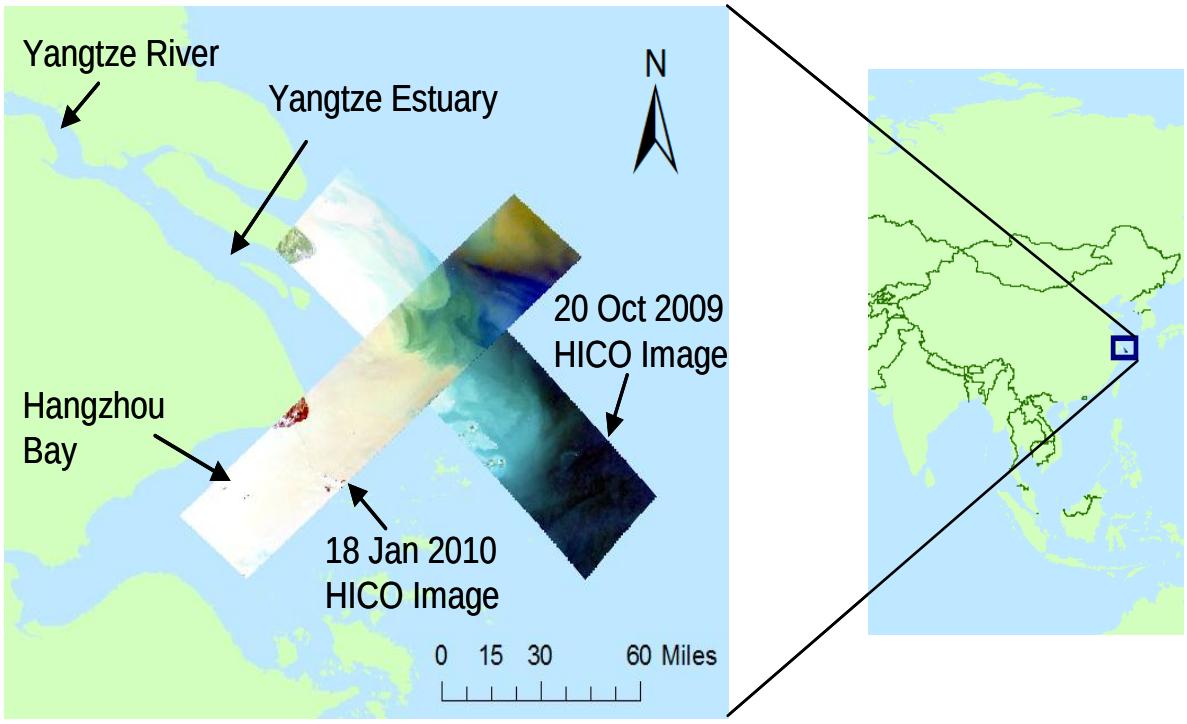

Figure 1: Map of the Yangtze Estuary and the Hangzhou Bay regions, with overlaid HICO images acquired on 20 October 2009 and 18 January 2010

For the purpose of algal bloom detection, because the chlorophyll-*a* algorithms require remote sensing reflectance, the at-sensor radiances from HICO were atmospherically corrected using the radiative transfer model Tafkaa (Gao *et al.*, 2000; Montes *et al.*, 2001).

Detection and Assessment of Sediment-loaded Plumes

Figure 2 shows a true color composite of the HICO image taken on 20 October 2009, a time when the river discharge undergoes its yearly decline The water flux and the sediment discharge are highly correlated to each other (Asanuma *et al.*, 2008), thus the spatial extent of the suspended sediments is largely confined to a region close to the coast, in contrast to the summer months when the discharge is high (the peak occurs in June) and the sediments are transported to offshore regions. The spatial patterns of the distribution of the suspended matter observed in the vicinity of the Yangtze Estuary are an outcome of the interactions among physical, chemical and biological factors (Ryu *et al.*, 2004). Considering the high nutrient transport through the Yangtze River (Chen *et al.*, 2003), the patchiness as observed in the HICO image shown in Figure 2 may also be indicative of the presence of plankton populations.

During non-flood seasons, the Yangtze River builds a salinity and turbidity front near 31°00'N, 122°30'E, as seen in the HICO image (Figure 2), which shows the front between the Yangtze Estuary and the offshore region. However, with increasing discharge from the Yangtze River, this front migrates farther east and can be found during flood seasons even beyond 123°E (Wang *et al.*, 2007).

The observed frontal system can be considered as an "ecological boundary," where towards the oceanic side, the water is clearer. Besides winds and coastal currents, upwelling in this region can also be driven by the centrifugal forces associated with strong tidal currents (Lu *et al.*, 2007).

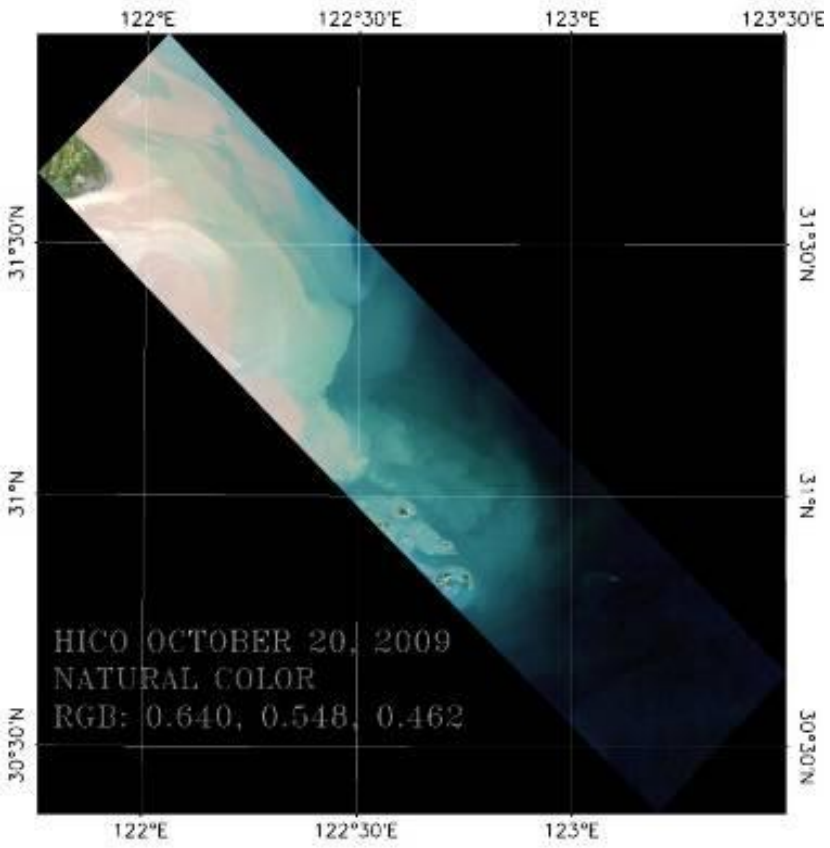

Figure 2: A true color composite of the HICO image acquired on 20 October 2009. The red, green, and blue spectral channels were centered at 0.64 µm, 0.548 µm, and 0.462 µm, respectively.

The entire HICO image acquired on 20 October 2009 was analyzed to identify the purest pixels using the Pure Pixel Index (PPI), a method to identify endmembers for spectral analysis which classifies the image based on the spectral angle (sensitive to the spectral shape) between endmember spectra, which are considered as n-dimensional vectors, where n is the number of bands and each pixel is a vector in n-dimensional space. For each endmember spectrum, a rule image was generated that contains the spectral angle between each pixel and the endmember spectrum. Smaller angles represent closer matches to the endmember spectrum. This technique, when used on radiometrically calibrated data, is insensitive to differences in the magnitude of the reflectances due to variations in illumination conditions and the surface albedo. The endmember spectra selected (Figure 3) were used as input for supervised classification. Considering the wavelength regions with the highest spectral difference among the endmember spectra, the spectral range for the input spectra was set to be from 0.451 µm to 0.703 µm.
The strong gradient between the Yangtze effluent and the adjacent water from the East China Sea can be recognized in Figure 4, which is a composite of three rule images from supervised classification. One rule image, which corresponded to a turbid endmember spectrum, shows a distinct plume formation. A subset of the rule image (Figure 5a) was density-sliced and examined further to study the structure of the plume. The density-sliced subset image shows the actual river effluent displayed in white, with adjacent patterns that are indicative of an algal bloom around the boundary between the river effluent and water from the East China Sea. Density slicing reveals a separate patch (shown in red on Figure 5b) in the upper part of the image, which is a region generally characterized by bloom conditions. The area beyond the regions shown in red, magenta and yellow, represent a front that seems to be caused by local upwelling.

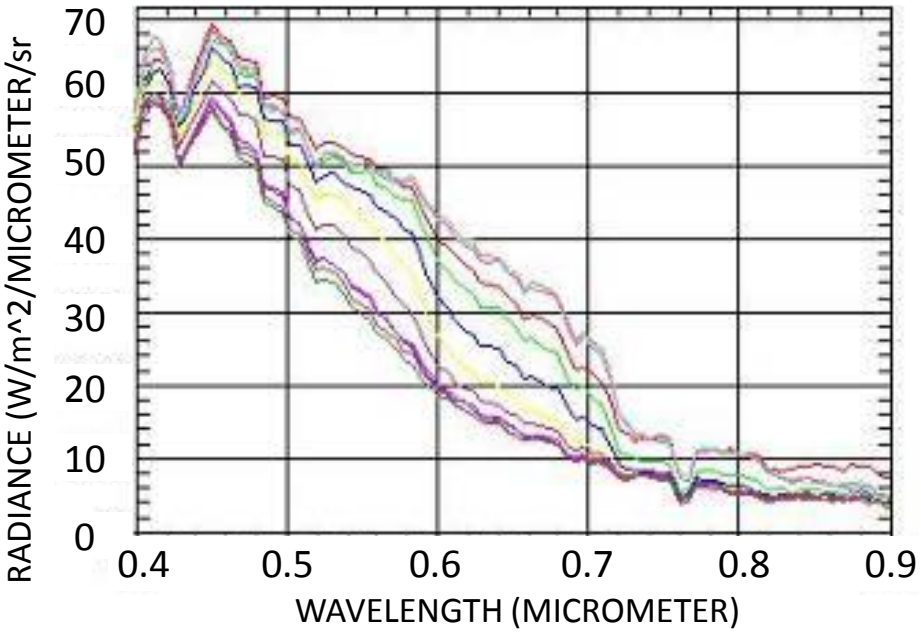

Figure 3: Endmember spectra at-sensor radiances from the HICO image obtained on 20 October 2009, which were selected based on the pure pixel indicator and used as input for spectral analysis.

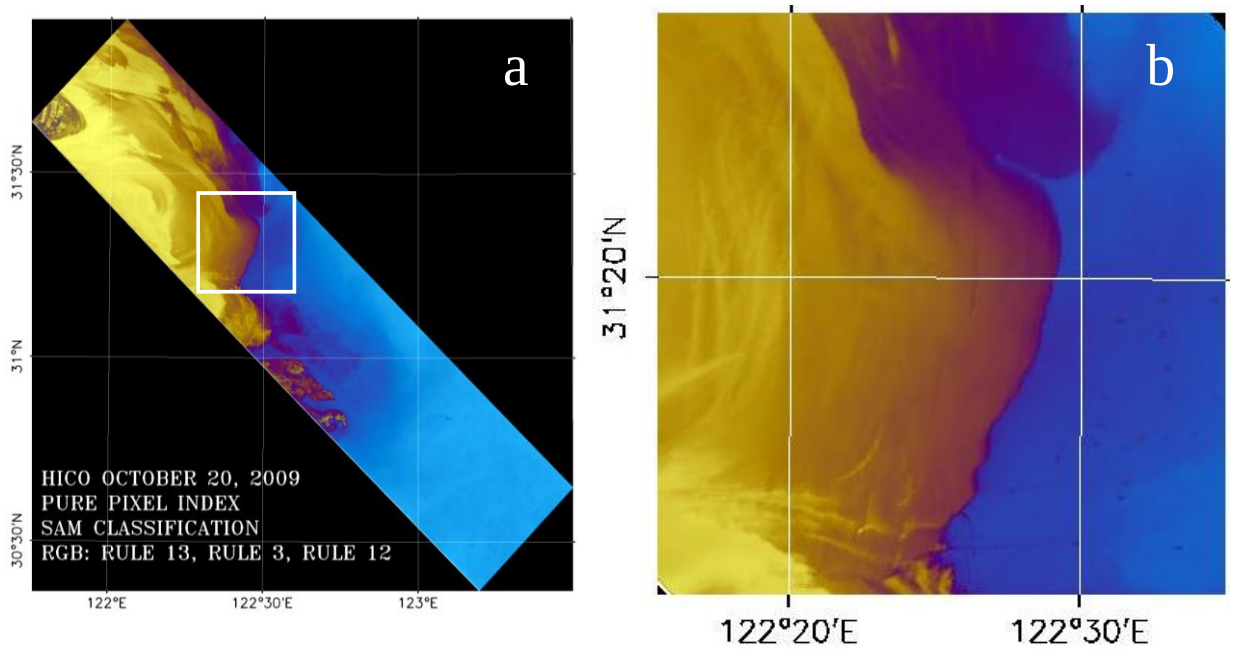

Figure 4: An RGB composite of three rule images derived from the HICO image acquired on 20 October 2009. Figure 4(b) is an enlarged view of the area within the white box in Figure 4(a), and shows spatial details at the edge of the plume.

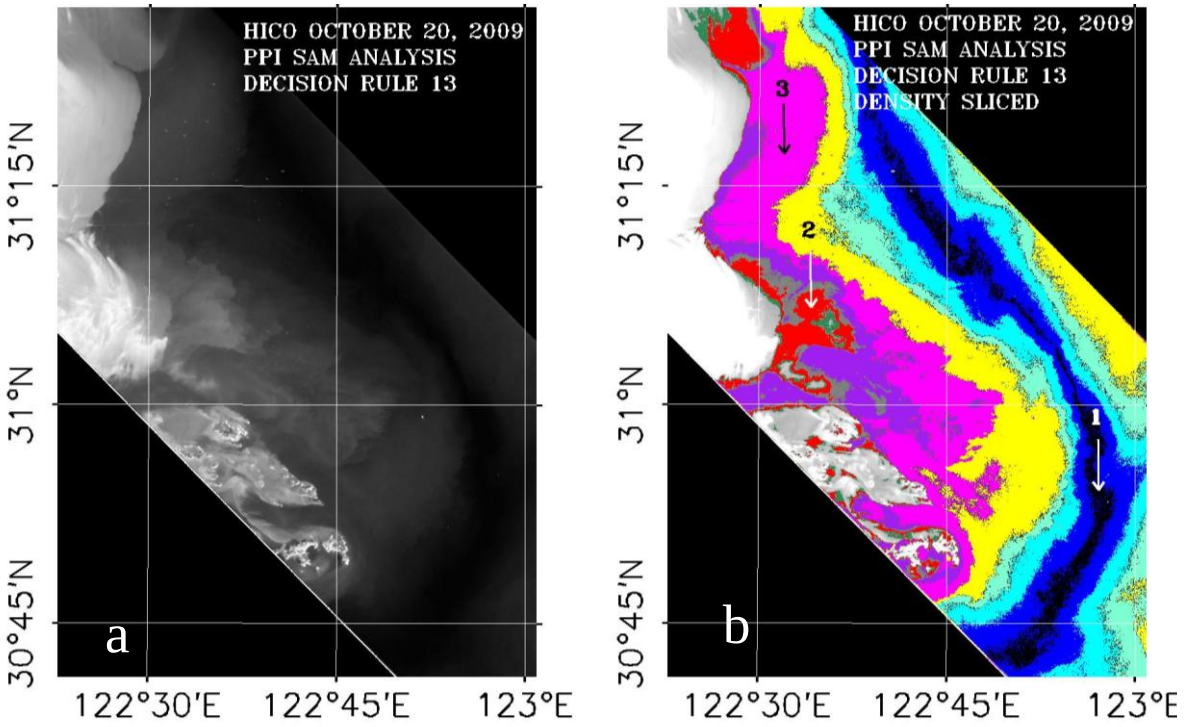

Figure 5: Decision rule image for the HICO image acquired on 20 October 2009 image, shown as (a) a gray scale image and (b) a density-sliced image, which shows an enhanced view of the structure of the dark front in Figure 5(a).

The presence of upwelling in the offshore water is supported by a study on upwelling in the Yangtze River estuary (Lu *et al.*, 2006). Although the research was conducted during the summer season, some conclusions are valid for other seasons as well. In principle, tidal mixing develops strong horizontal density gradients that result in fronts at the surface. Upwelling is a result of bottom currents ascending upward and regulating the location and intensity of tidal fronts. However, one has to take into consideration that, aside from tides and bathymetry, the Yangtze River discharge and the intensity of the Taiwan Warm Current also locally alter the strength of upwelling (Lu *et al.*, 2006).

HICO revisited a part of the East China Sea on 18 January 2010, but covered only a portion of the offshore area that was covered on 20 October 2009. However, the image contained a good coverage of the Hangzhou Bay, which is hydrographically also influenced by the effluent water and sediment transport from the Yangtze River. The variable density flow of water at the plume front in the bay plays a key role in dispersing the fine, suspended sediments from the Yangtze River southward during non-flood seasons(Chen *et al.*, 2003). In order to characterize the gradient of the suspended sediments through spectral analysis, endmember spectra were extracted from regions of sediment patches that were visually identified from the true color composite (Figure 6).

The highest magnitudes of at-sensor radiance (spectra 1 and 2 in Figure 6a) were found in the inner part of the Hangzhou Bay and corresponded to high concentrations of suspended matter. Due to the fact that the Bay has an average depth of only about 10 m, sediments that are mainly composed of fine and medium silt are easily re-suspended (Su and Wang, 1989). The at-sensor radiance was lower in magnitude

in the offshore region (Figure 6), especially in the wavelength region between 0.5 µm and 0.75 µm, where the water-leaving radiance is significantly affected by scattering of light by suspended sediments.

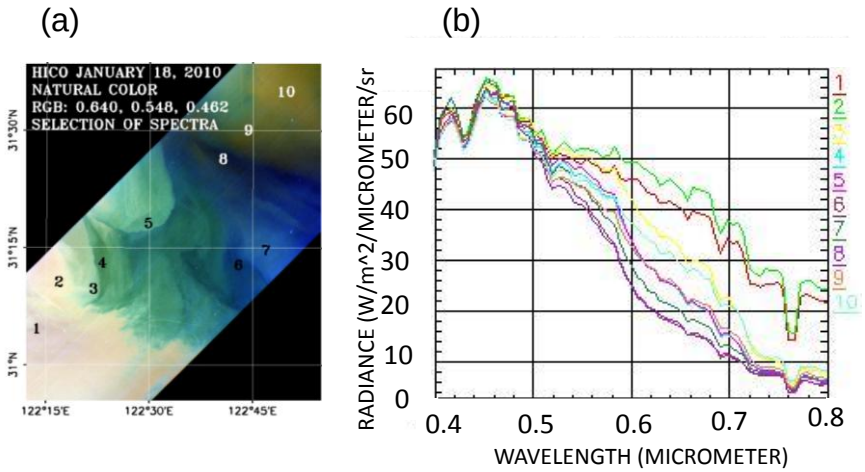

Figure 6: (a) A true color composite of a subset of the HICO image acquired on 18 January 2010; (b) endmember spectra (at-sensor radiances) selected for supervised classification.

The spectral range from 0.451 µm to 0.703 µm was used for multispectral analysis of the image acquired on 18 January 2010. Figure 7 contains three individual rule images and a composite of the three rule images. The results clearly show the region with high suspended matter in the Hangzhou Bay. In addition, a front that defines the boundary of the Yangtze River effluent can also be identified close to the center of the image. The area displayed in magenta in Figure 7d is known to be an upwelling region (Pei *et al.*, 2009) and is presumed to be under algal bloom conditions.

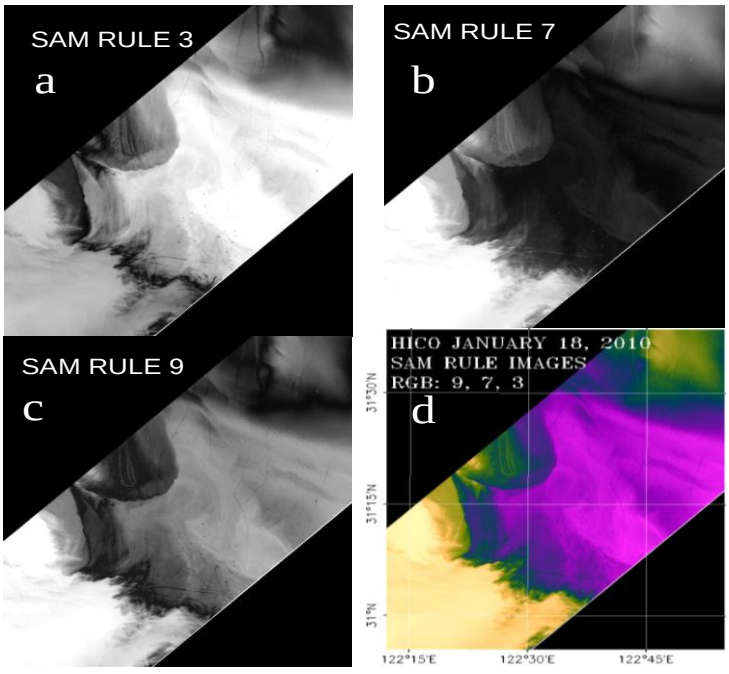

Figure 7: Three rule images, (a), (b) and (c), and the corresponding RGB composite image (d) for the HICO image acquired on 18 January 2010.

Research Article

Detection of Algal Bloom Conditions

Detection of possible algal bloom development close to the estuary was carried out with multispectral analysis of the image acquired on 20 October 2009. The input endmember spectra and their pixel locations are shown in Figure 8. The dark blue region seen in Figure 8c represents a distinct patch in the estuary. The Yangtze River Estuary is marked by a strong gradient that separates the river effluent from the neighboring ocean water. The image was taken in October and it is still likely that increased algal concentration may have caused the patchiness observed outside the strong frontal system. A color composite of rule images (Figure 8d) suggests the development of an algal bloom along the effluent gradient. Previous studies (Shanmugam *et al.,* 2008) have reported the existence of algal patches in this region throughout the year even though the spatial pattern and the intensity of the frontal system may fluctuate. Song *et al.,* (2008) also have reported the occurrence of similar bloom conditions in this region in 2004.

The aforementioned observations can be confirmed with chl-*a* estimates obtained by applying an ocean color algorithm (O'Reilly *et al.,* 2000) to HICO data (Figure 9). The HICO image acquired on 20 October 2009 was atmospherically corrected prior to the application of the algorithm. Elevated chl-*a* concentrations were found outside the strong boundary between the Yangtze River effluent and the adjacent water of the East China Sea. As chlorophyll algorithms are not reliable for very turbid and productive waters (Carder *et al.,* 2004; Dall'Olmo *et al.,* 2005; Darecki and Stramski, 2004) the chl-*a* estimation was restricted only to areas where the retrieved chl-*a* concentration was less than 4 mg m^{-3}, and only qualitative inferences were made from the retrieved chl-*a* concentrations. The highest estimated chl-*a* concentrations (3.5 – 4.0 mg m^{-3}) were found mainly in the Yangtze Estuary. For comparison, it should be mentioned that Song *et al.,* (2008) reported high chl-*a* concentrations (2 – 8 mg m^{-3}) in this region in 2004. Lower chl-*a* concentrations (0.5 – 1 mg m^{-3}) were observed in the southeast direction farther away from the estuary.

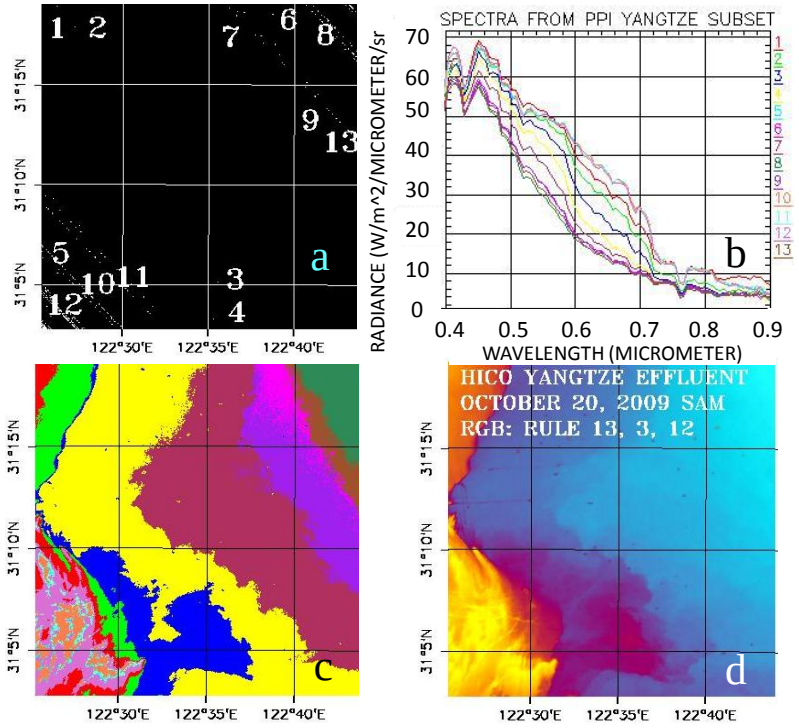

Figure 8: Spectral analysis of the 20 October 2009 image: (a) pixel locations of the endmember spectra (b) endmember spectra; (c) rule image displayed using an inverted color table; (d) RGB composite of three rule images.

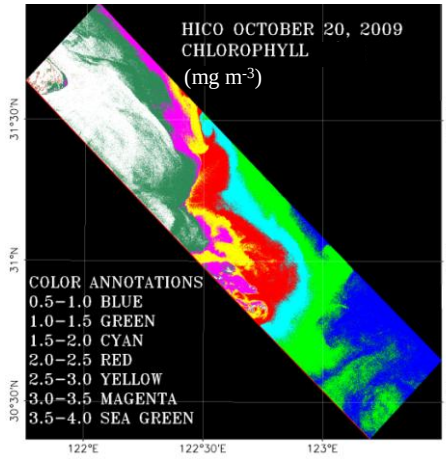

Figure 9: Chl-*a* concentrations around the Yangtze Estuary, estimated from the atmospherically corrected HICO image acquired on 20 October 2009.

Chl-*a* concentrations were also estimated from the same HICO image acquired on 18 January 2010. Figure 10 shows the estimated chl-*a* concentrations for the Hangzhou Bay and the adjacent boundary that separates the highly turbid estuarine water from the oceanic water of the East China Sea. Chl-*a* concentrations ranged from 1 mg m^{-3} to 4 mg m^{-3} in the region outside the turbidity front that was previously identified using spectral analysis. The lighter green and white areas towards the Hangzhou Bay correspond to regions that were identified in the analysis as waters with high suspended sediment concentrations. As with the 20 October 2009 image, chl-*a* estimation was restricted to areas where the retrieved chl-*a* concentration was less than 4 mg m^{-3}. The white areas represent pixels for which the retrieved chl-*a* concentration was above 4 mg m^{-3}. A comparison was made with a MODIS image acquired on 18 January 2010, covering the Yangtze Estuary and the Hangzhou Bay, as shown in Figure 10a. This comparison between the chl-*a* estimates from the HICO image and the MODIS image revealed similar patterns of chl-*a* distribution (Figures 10b and 10c).

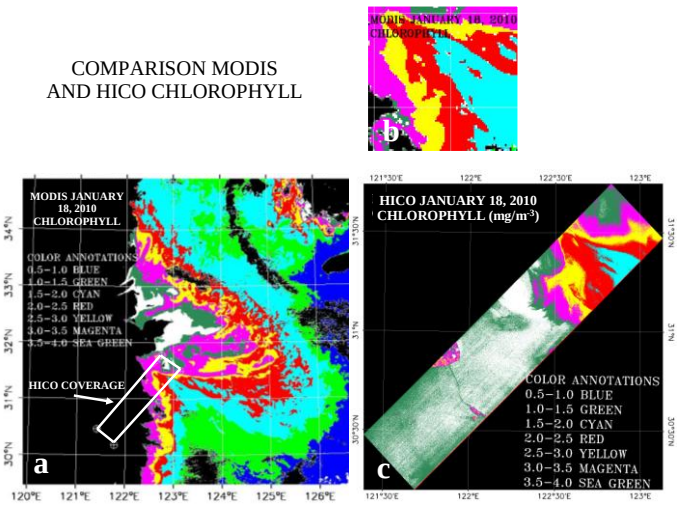

Figure 10: Estimated chl-*a* concentrations for 18 January 2010: (a) chl-*a* estimates from the MODIS image; (b) chl-*a* estimates from the MODIS image for the area that overlapped with the HICO image; (c) chl-*a* estimates from the HICO image (the white areas represent pixels with chl-*a* concentration above 4 mg m^{-3}).

CONCLUSION

This study was carried out in the Yangtze River discharge region and Hangzhou Bay in the East China Sea where there is a significant discharge of sediment and high levels of nutrients as a result of anthropogenic activities. The interaction of water from the Yangtze River and the adjacent Hangzhou Bay with the water from the East China Sea, and the complex patterns that ensue, lead to fronts and algal blooms in the East China Sea.

Within the Yangtze River plume, the suspended sediments result in an estimated photon penetration depth of less than 3 m (Luan *et al.*, 2006). In consequence, light penetration into the water is likely the primary limiting factor for primary production, even though high levels of nutrients might be available from anthropogenic sources and natural recycling of nutrients. In areas adjacent to the fronts in the East China Sea, elevations in chl-*a* concentrations which were considered as plankton patches and were confirmed with estimates of chl-*a* concentration, were obtained from atmospherically corrected HICO data. Fronts recognized with HICO data in areas adjacent to the Yangtze River Estuary and the Hangzhou Bay were also interpreted as areas of high chl-*a* concentration. This was confirmed by chl-*a* concentrations estimated from atmospherically corrected HICO data, which showed values of around 3 mg m^{-3} for this region.

ACKNOWLEDGMENT

This work was supported by grants from the Office of Naval Research, the American Society for Engineering Education Summer Senior Faculty Fellowship awarded to K. H. Szekielda, and the National Research Council Research Associateship awarded to W. J. Moses, via the Naval Research Laboratory.

REFERENCES

Asanuma I, Zhu J, Zhao C, Huang B and Xu Q (2008). Contribution of the Yangtze River to ecosystem of the East China Sea. *The International Archives of the Photogrammetry, Remote Sensing and Spatial Information Sciences* **XXXVII**(B8), Commission VIII, WG VIII/6, Beijing 669-672.

Bissett PW, Arnone RA, Davis CO, Dickey TD, Dye D, Kohler DDR and Gould RW (2004). From meters to kilometers – a look at ocean color scales of variability, spatial coherence, and the need for fine scale remote sensing in coastal ocean optics. *Oceanography* **17**(2) 32-43.

Carder KL, Chen FR, Cannizzaro JP, Campbell JW and Mitchell BG (2004). Performance of the MODIS semi-analytical ocean color algorithm for chlorophyll-a. *Advances in Space Research* **33**(7) 1152-1159.

Chai C, Yu Z, Song S and Cao X (2006). The Status and Characteristics of Eutrophication in the Yangtze River (Changjiang) Estuary and the Adjacent East China Sea, China. *Hydrobiologia* **563**(1) 313-328.

Chang G, Mahoney K, Briggs-Whitmire A, Kohler DDR, Mobley CD, Lewis M, Moline MA, Boss E, Kim M, Philpot W and Dickey TD (2004). The New Age of Hyperspectral Oceanography. *Oceanography* **17**(2) 16-23.

Chen C, Zhu J, Beardsley RC and Franks JPS (2003). Physical–biological sources for dense algal blooms near the Yangtze River. *Geophysical Research Letters* **30**(10) 1513.

Dall'Olmo G, Gitelson AA, Rundquist DC, Leavitt B, Barrow T and Holz JC (2005). Assessing the potential of SeaWiFS and MODIS for estimating chlorophyll concentration in turbid productive waters using red and near-infrared bands. *Remote Sensing of Environment* **96**(2) 176-187.

Darecki M and Stramski D (2004). An evaluation of MODIS and SeaWiFS bio-optical algorithms in the Baltic Sea. *Remote Sensing of Environment* **89**(3) 326-350.

Davis CO, Kavanaugh M, Letelier R, Bissett PW and Kohler D (2007). Spatial and Spectral Resolution Considerations for Imaging Coastal Waters. *Proceedings SPIE, Characterization and Variability of the Coastal Ocean: Composition and Bio-Optical Properties II* **6680** 66800.

Gao BC, Montes MJ, Ahmad Z and Davis CO (2000). Atmospheric correction algorithm for hyperspectral remote sensing of ocean color from space. *Applied Optics* **39**(6) 887-896.

Hickox R, Belkin I, Cornillon P and Shan Z (2000). Climatology and Seasonal Variability of Ocean Fronts in the East China, Yellow and Bohai Seas from Satellite SST Data. *Geophysical Research Letters* **27**(18) 2945-2948.

Korwan DR, Lucke RL, Corson M, Bowles JHGao BC, Li RR, Montes MJ, Snyder WA, McGlothlin NR, Butcher SD, Wood DL, Davis CO and Miller WD (2010). The Hyperspectral Imager for the Coastal Ocean (HICO) – design and early results. In *IGRSS Workshop on Hyperspectral Image and Signal Processing: Evolution in Remote Sensing* (IEEE, 2010) 1-4.

Limeburger R, Beardsley RC and Zhao JS (1983). Water masses and circulation in the East China Sea. *Proceedings of the International Symposium on Sedimentation on the Continental Shelf*, China Ocean Press, Beijing 261-269.

Lü X, Qiao F, Xia C and Yuan Y (2007). Tidally induced upwelling off Yangtze River estuary and in Zhejiang coastal waters in summer. *Science in China Series D* **50**(3) 462-473.

Lü X, Qiao F, Xia C and Yuan Y (2006). Upwelling off Yangtze River estuary in summer. *Journal of Geophysical Research* **111**.

Luan Q, Sun J, Shen Z, Song S and Wang M (2006). Phytoplankton Assemblage of Yangtze River Estuary and the Adjacent East China Sea in Summer, 2004. *Journal of Ocean University of China* (English edition) **5**(2) 123-131.

Lucke RL, Corson M, McGlothlin NR, Butcher SD, Wood DL, Korwan DR, Li RR, Snyder WA, Davis CO and Chen DT (2011). Hyperspectral Imager for the Coastal Ocean: instrument description and first images. *Applied Optics* **50**(11) 1501-1516.

Montes MJ, Gao BC and Davis CO (2001). A new algorithm for atmospheric correction of hyperspectral remote sensing data. *Proceedings of SPIE, Geo-Spatial Image and Data Exploitation II*, edited by Roper WE **4383** 23-30.

Moses WJ, Gitelson AA, Berdnikov S and Povazhnyy V (2009). Estimation of chlorophyll-*a* concentration in case II waters using MODIS and MERIS data—successes and challenges. *Environment Research Letters* **4**(045005) 8.

O'Reilly JE *et al.*, (2000). SeaWiFS Postlaunch Calibration and Validation Analyses, Part 3, *NASA Technical Memorandum 2000-206892* **11** 49.

Pei S, Shen Z and Laws EA (2009). Nutrient Dynamics in the Upwelling Area of Changjiang (Yangtze River) Estuary. *Journal of Coastal Research* **25**(3) 569-580.

Ryu JH, Ahn YH and Shanmugam P (2004). Monitor spatial and temporal patterns of suspended sediments in the East China and Yellow Seas using SeaWifs data. *Gayana (Concepción)* **68**(2) 514-519.

Shanmugam P, Ahn Y-H and Ram PS (2008). SeaWiFS sensing of hazardous algal blooms and their underlying mechanisms in shelf-slope waters of the Northwest Pacific during summer. *Remote Sensing of Environment* **112**(7) 3248-3270.

Shen HT, Li JF, Zhu HF, Han MB and Zhou FO (1983). Transport of the suspended sediments in the Changjiang Estuary. *Proceedings of the International Symposium on Sedimentation on the Continental Shelf*, China Ocean Press, Beijing 359-369.

Son S, Yoo S and Noh JH (2006). Spring Phytoplankton Bloom in the Fronts of the East China Sea. *Ocean Science Journal* **41**(3) 181-189.

Song S, Sun J, Luan Q and Shen Z (2008). Size-fractionated phytoplankton biomass in autumn of the Changjiang (Yangtze) River Estuary and its adjacent waters after the Three Gorges Dam construction. *Chinese Journal of Oceanology and Limnology* **26**(3) 268-275.

Su J and Wang K (1989). Changjiang river plume and suspended sediment transport in Hangzhou Bay. *Continental Shelf Research* **9(**1) 93-111.

Sydor M, Gould RW, Arnone RA, Haltrin VI and Goode W (2004). Uniqueness in remote sensing of the inherent optical properties of ocean water. *Applied Optics* **43**(10) 2156-2162.

Szekielda KH and McGinnis D (1991). Spatial Variability of River Plumes and Eutrophication. In: *Biogeochemistry of Major World Rivers*, edited by Degens ET, Kempe S and Richey JE, John Wiley and Sons, Inc. Chichester, U.K. 1-24.

Wang Z, Li L, Chen D, Xu K, Wei T, Gao J, ZhaoY , Chen Z and Masabate W (2007). Plume front and suspended sediment dispersal off the Yangtze (Changjiang) River mouth, China during non-flood season. *Estuarine, Coastal and Shelf Sciience* **71** 60-67.

Wang M and Shi W (2005). Estimation of ocean contribution at the MODIS near-infrared wavelengths along the east coast of the U.S.: Two case studies. *Geophysical Research Letters* **32** L13606.

Yan SZ and Hu FX (1986). Characteristics of minerals in Qiantangjiang Estuary and its relationship with the hydrodynamic environment (in Chinese), *Journal of the East China Normal University* **4** 83-90.

Zheng Q and Klemas V (1982). Determination of winter temperature patterns, fronts and surface currents in the Yellow Sea and East China Sea from satellite imagery. *Remote Sensing of Environment* **12** 201-218.